



Unexpectedly efficient CO₂ hydrogenation to higher hydrocarbons over non-doped Fe₂O₃



Matthias Albrecht^a, Uwe Rodemerck^a, Matthias Schneider^a, Martin Bröring^b,
Dirk Baabe^b, Evgenii V. Kondratenko^{a,*}

^a Leibniz-Institut für Katalyse e.V., Albert-Einstein-Str. 29a, 18059 Rostock, Germany

^b Institut für Anorganische und Analytische Chemie, Technische Universität Braunschweig, Hagenring 30, 38106 Braunschweig, Germany

ARTICLE INFO

Article history:

Received 12 August 2016

Received in revised form 20 October 2016

Accepted 10 November 2016

Available online 11 November 2016

Keywords:

Iron oxide

CO₂ hydrogenation

Fischer-Tropsch

Preparation method

ABSTRACT

Since CO₂ hydrogenation into higher hydrocarbons is an attractive approach to mitigate greenhouse effect and to reduce reliance on fossil feedstock, this reaction has been intensively studied over Fe-based catalysts. They had, however, to be promoted with oxides of e.g. K, Cu, Mn and/or Ce to reduce undesired CH₄ formation and to increase olefin selectivity. Here, we demonstrate, for the first time, that similar improvements can be achieved without using dopants but by preparing bare Fe₂O₃ according to a template-assisted synthesis method. Under optimized reaction conditions (total pressure of 15 bar, 623 K and H₂/CO₂ = 3/1), the selectivity to C₂–C₄ hydrocarbons with the olefin to paraffin ratio of 2.7 was about 37% at CO₂ conversion of 40%, while the selectivity to C₅₊ hydrocarbons, CH₄ and CO was around 36, 12 and 15% respectively. Our thorough characterization study with complementary techniques (H₂-TPR, XRD, and Mössbauer spectroscopy) enabled us to conclude that this preparation method affects reducibility of Fe₂O₃ and, thus, its ability for *in situ* transformation into catalytically active iron carbide(s) under CO₂-hydrogenation conditions.

© 2016 Elsevier B.V. All rights reserved.

1. Introduction

An issue of major current concern is the effect of human activities on steadily increasing concentration of greenhouse gases in the atmosphere and the resulting global warming, which can eventually lead to natural disasters such as floods, hurricanes, and droughts [1]. Carbon dioxide formed from fossil fuels is up to 26% responsible for the greenhouse effect [2] and is the greatest man-made factor. Therefore, reducing CO₂ emissions into the atmosphere is of enormous environmental interest. This can be achieved by either its capture/storage [3–5] or utilization as a reactant for producing fuels and useful chemicals in an environmentally friendly manner. The latter option appears to be more attractive because it opens an alternative raw-material source to the currently used crude oil and natural gas. As a result, CO₂ conversion into various chemicals gained importance both in academia and industrial research using homogeneous, heterogeneous, photo or electro catalysts as documented in several recent reviews on the topic [6–15]. There are already successful examples of commercially

available technologies for one-step CO₂ conversion into methanol or methane [16–18]. Another approach under investigation is CO₂ hydrogenation to synthetic fuels, *i.e.* CO₂ Fischer-Tropsch (CO₂-FT) synthesis [19,20].

It is in general accepted that CO₂-FT synthesis consists of two main consecutive reactions: reverse water gas shift (RWGS) reaction to CO followed by hydrogenation of the latter to hydrocarbons according to the classical FT synthesis. Owing to the ability of Fe-based materials to catalyze both of these reactions, such catalysts are traditionally used in CO₂-FT [21–24]. They are used in form of bulk [25–29] or supported iron oxides [30–37]. To reduce CH₄ selectivity (non-desired reaction product), catalysts are typically doped with oxides of K, Cu, Mn and/or Ce. The dopants affect the reducibility of FeO_x species, their distribution, and overall catalyst basicity. While the effects of dopants have been explored for many years, little effort was made in improving the performance of non-doped iron oxide through its proper synthesis. The target material property to be affected by the preparation method could be reducibility of Fe₂O₃ because this oxide must be *in situ* transformed into iron carbides, which are considered to be catalytically active and selective species [38–40]. In our previous studies, a cellulose-templated method was demonstrated to be a suitable technique for tuning redox properties of catalysts on the basis of Al₂O₃ [41] and CeO₂

* Corresponding author.

E-mail address: evgenii.kondratenko@catalysis.de (E.V. Kondratenko).

[42]. These materials showed superior performance in comparison to their classically prepared counterparts in partial oxidation of methane to syngas.

In the present contribution, we explore the potential of the above method for preparation of Fe_2O_3 catalysts with reduced selectivity to CH_4 in favor of C_{2+} hydrocarbons and in particular high fraction of $\text{C}_2\text{--}\text{C}_4$ olefins in CO_2 -FT synthesis. The effect of calcination conditions on physico-chemical and catalytic properties of so-prepared materials was also investigated. The materials in their fresh and spent forms were systematically investigated by XRD, H_2 -TPR, and Mössbauer spectroscopy. For highlighting the importance and the potential of synthesis method for designing selective catalysts, we compared catalytic performance of our catalysts with that of the state of the art Fe-based catalysts, which are either supported or bulk materials, however, doped with various promoters for improving catalyst performance [27,28,30,33,35,36]. Finally, optimizing reaction conditions such as pressure, temperature, and reactant feed composition revealed how and which further improvements in selectivity to desired products and in CO_2 conversion can be achieved.

2. Experimental

2.1. Catalyst preparation

Three Fe_2O_3 samples were prepared from $\text{Fe}(\text{NO}_3)_3 \cdot 9\text{H}_2\text{O}$ (99%, Fisher) according to the following protocols. The $\text{Fe}_2\text{O}_3\text{-P}$ was synthesized by precipitation from an aqueous solution of the above precursor. Briefly, 50 g of iron nitrate were dissolved in 1.5 L water followed by adding 30 g of urea ($\geq 99\%$, Roth). Hereafter, the solution was heated to 368 K and tempered under continuous stirring for 24 h. The resulting solid was filtered and washed several times. Calcination was carried out in a flow of air at 873 K for 6 h. W542 cellulose fibers provided by WhatmanTM were used as template for $\text{Fe}_2\text{O}_3\text{-CT}$ preparation according to [43,44]. An aqueous solution (1 mol/L) of iron nitrate was fully absorbed by the template at room temperature (around 298 K). The wet template was then transferred into a muffle furnace preheated to 873 K or 1173 K to yield $\text{Fe}_2\text{O}_3\text{-CT600}$ and $\text{Fe}_2\text{O}_3\text{-CT900}$ materials respectively. A membrane pump was used to provide synthetic air to the furnace for supporting combustion process of the cellulose template. The samples were calcined at the respective temperature for 6 h. Both temperature-programmed oxidation and elemental analysis tests proved that the calcined samples contain only trace amounts (well below 1 wt.%) of residual carbon. Thus, we can safely conclude that our materials are bulk iron oxide(s) and not supported on carbon.

2.2. Catalyst characterization

Both, fresh and spent Fe_2O_3 materials were thoroughly characterized by various but complementary techniques.

Nitrogen adsorption-desorption isotherms for each catalyst were collected at 77 K on a BELSORP-mini II (BEL Japan, Inc.) setup. The specific surface area was calculated from the adsorption isotherm applying the Brunauer, Emmett, and Teller equation for the N_2 relative pressure range of $0.05 < P/P^0 < 0.30$.

Reducibility of fresh samples was investigated by temperature-programmed reduction (TPR) in an in-house developed set-up equipped with eight individually heated continuous-flow fixed-bed tubular (length, outer and inner diameters were 240, 9, and 7 mm respectively) quartz reactors. In these experiments, 8 mg of each catalyst were heated in an H_2 flow (5 vol.% H_2 in Ar) of 20 mL/min to 1173 K with a constant heating rate of 10 K/min. The product gas flow was analyzed by an on-line mass spectrometer (Pfeiffer OmniStar GSD 300 01). The following atomic mass units were ana-

lyzed: 40 (Ar), 18 (H_2O), and 2 (H_2). The concentration of hydrogen was determined from the respective atomic mass unit by using the sensitivity factor determined by analyzing calibration gas mixtures.

To identify the phase composition of fresh and spent samples, powder X-ray diffraction (XRD) measurements were performed on a Theta/Theta diffractometer X'Pert Pro (Panalytical) with Cu $\text{K}\alpha$ radiation and an X'Celerator RTMS detector. The alignment of XRD reflexes was made according to a silicon standard. The data were collected at room temperature in the 2 Theta range from 5 to 80°. The phase composition of the samples was determined using the program suite WinXPOW (Stoe & Cie) with inclusion of the powder diffraction file PDF2 of the international center of diffraction data. Scherrer equation was used for the 3 strongest reflexes of each diffractogram belonging to a certain phase to calculate the size of crystallites.

^{57}Fe -Mössbauer spectroscopic measurements were performed on a standard transmission spectrometer with sinusoidal velocity sweep. The measurements on polycrystalline specimens of $\text{Fe}_2\text{O}_3\text{-CT600}$ (fresh and spent) were done with a Janis closed-cycle cryostat with He exchange gas at temperatures between 20 and 300 K. The activity of the Mössbauer source was about 6 mCi of ^{57}Co in a Rh matrix kept at ambient temperature. The sample temperature was recorded with a calibrated Si diode located close to the sample container made of Teflon or PEEK. The measurements on polycrystalline samples of $\text{Fe}_2\text{O}_3\text{-P}$ and $\text{Fe}_2\text{O}_3\text{-CT900}$ (fresh and spent) were carried out on a CryoVac continuous flow cryostat with comparable specifications, geometry, and sample environment as described above. The activity of the Mössbauer source used here was about 25 mCi of ^{57}Co in a Rh matrix. The recorded Mössbauer spectra were analyzed using a standard least-squares fitting routine with sextets of Lorentzian lines. The isomer shift δ is reported with respect to iron metal at ambient temperature and was not corrected in terms of second order Doppler shift.

2.3. Catalytic tests

Catalytic tests were performed in an in-house developed setup equipped with 50 continuous-flow fixed-bed stainless-steel tube (length, outer and inner diameters were 230, 6, and 4 mm respectively) reactors operating in parallel. The reactors were located in one electrically heated furnace equipped by a fan for a proper heat distribution. In a typical experiment, 300 mg of catalyst (250–450 μm fraction) were filled into each reactor. 700 mg of SiC (ESK-SiC, 500–710 μm fraction) were additionally added on the top of the catalyst layer to achieve plug flow and to preheat feed gases. An in-house developed flow restrictor equally distributed the total gas flow to 50 reactors with a desired and constant flow through each reactor. CO_2 , H_2 , and N_2 were dosed by electronic mass flow controllers (Brooks 5850s).

Before starting CO_2 -hydrogenation tests, the catalysts were reduced at 773 K and 10 bar in a flow (11.8 mL/min per reactor) of $\text{H}_2/\text{N}_2 = 1/1$ for 2 h. After cooling down in this flow to the reaction temperature of 573 K, a mixture of H_2 , CO_2 , and N_2 with the ratio of $\text{H}_2/\text{CO}_2/\text{N}_2 = 3/1/0.3$ was fed with a flow rate of 5.7 mL/min per reactor. Additional experiments were performed in a similar way to investigate the effect of temperature (523, 573, 623 and 673 K), pressure (10 and 15 bar) and feed composition ($\text{H}_2/\text{CO}_2 = 3/1$ and $\text{H}_2/\text{CO}_2 = 6/1$).

To investigate the effect of CO_2 conversion on product selectivity, we performed tests at different GHSV (gas hourly space velocity). This was achieved by varying catalyst amount (300, 100, 50, 30, 20, 10 and 5 mg) whereas total feed flow rate amounted to 5.7 mL/min per reactor. Regardless of the catalyst amount, a layer of 700 mg SiC was added on top. These tests were carried out with a $\text{H}_2/\text{CO}_2/\text{N}_2 = 6/1/0.3$ feed at 623 K and total pressure of 15 bar. We report catalytic results after achieving a steady-state operation at

Table 1 S_{BET} values and phase composition of fresh and spent catalysts.

Catalysts	$S_{\text{BET}}/\text{m}^2/\text{g}$		XRD analysis		Mössbauer spectroscopy	
	fresh	spent ^a	fresh	spent ^a	fresh	spent ^a
Fe ₂ O ₃ .P	30	10	Fe ₂ O ₃	Fe ₃ O ₄	α -Fe ₂ O ₃	Fe ₃ O ₄ (72%), χ -Fe ₅ C ₂ (28%)
Fe ₂ O ₃ .CT600	5	2	Fe ₂ O ₃	Fe ₃ O ₄ , Fe ₅ C ₂	α -Fe ₂ O ₃	β -FeO(OH) (19%), Fe carbides (81%)
Fe ₂ O ₃ .CT900	1	<1	Fe ₂ O ₃	Fe ₃ O ₄	α -Fe ₂ O ₃	Fe ₃ O ₄ (73%), α -Fe (6%), χ -Fe ₅ C ₂ (21%)

^a After 120 h on stream; T = 623 K, P = 15 bar, H₂/CO₂/N₂ = 6/1/0.3, F/m_{cat} = 1140 mL/(g h).

each GHSV. Such condition was typically achieved after around 4 h on stream.

The feed components and the reaction products were analyzed by an on-line gas chromatograph (Agilent 7890A) equipped with PLOT/Q (for CO₂), AL/S (for hydrocarbons C₁–C₈), DB-FFAP (for higher hydrocarbons, i.e. C₉–C₁₈), and Molsieve 5 (for H₂, O₂, N₂, and CO) columns as well as flame ionization and thermal conductivity detectors. To avoid condensation of higher hydrocarbons, stainless steel lines between the reactor outlet and the GC inlet were heated to around 200 °C.

The conversion (X) of CO₂, product yield (Y) and selectivity (S) were calculated according to Eqs. (1)–(3) respectively.

$$X_{\text{CO}_2} = 1 - \frac{\dot{n}_{\text{CO}_2}^{\text{outlet}}}{\dot{n}_{\text{CO}_2}^{\text{inlet}}} \quad (1)$$

$$Y_i = \frac{a_i \cdot \dot{n}_i^{\text{outlet}}}{\dot{n}_{\text{CO}_2}^{\text{inlet}}} \quad (2)$$

$$S_i = \frac{Y_i}{X_{\text{CO}_2}} \quad (3)$$

where \dot{n}_i and a_i stand for molar flows of component *i* and number of carbon atoms in this component respectively. Subscripts “inlet” and “outlet” are used for distinguishing between inlet and outlet molar flows. The inlet molar flows of feed components were determined through separate measurements using a bypass line. The change in

gas volume during reaction was taken into account via correction of the measured peak areas with N₂ as an internal standard.

Chain growth probability α was determined in an approach, where the decimal logarithm of molar fractions of formed hydrocarbons (C₁–C₈) is plotted versus their carbon number. The slope *m* of the resulting plot is used for calculating α according to Eq. (4).

$$\alpha = 10^m \quad (4)$$

3. Results and discussion

3.1. Physico-chemical catalyst characterization

3.1.1. Surface and bulk properties

The specific surface area (S_{BET}) of fresh and spent materials is listed in Table 1. Among the fresh materials, the highest S_{BET} of 30 m²/g was determined for Fe₂O₃.P. The corresponding values for Fe₂O₃.CT600 and Fe₂O₃.CT900 were 5 and 1 m²/g. The lowest S_{BET} for the latter material is due to the fact that it was calcined at the highest temperature of 1173 K. After performing CO₂ hydrogenation at 623 K for 120 h, the specific surface area of all the catalysts tested significantly decreased, thus indicating reaction-induced catalyst restructuring.

The preparation method was also established to influence the morphology of catalyst particles. While Fe₂O₃ obtained from iron nitrate through a precipitation method consists of spheroids, the CT-prepared Fe₂O₃ comprises fibers replicating the pore structure of the template material (Figs. S1 and S2). The morphology of the

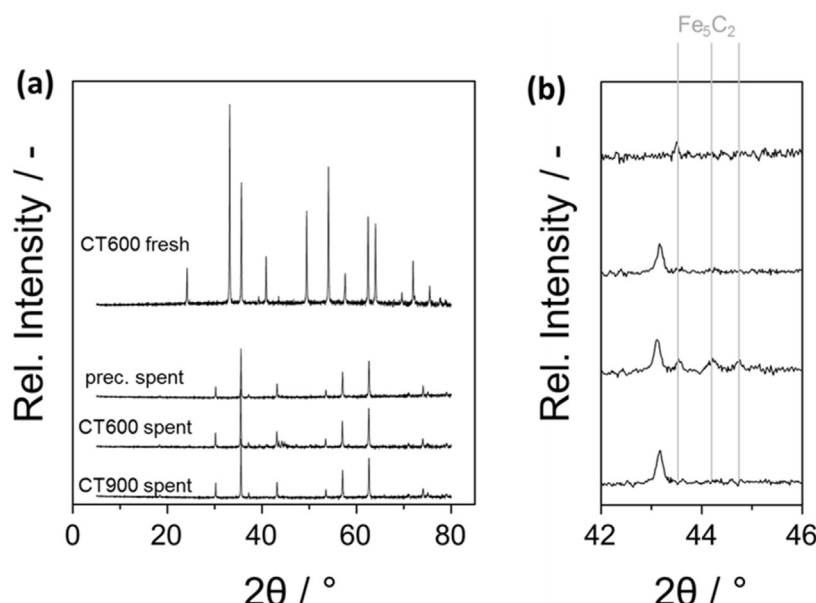


Fig. 1. X-ray diffractograms of fresh Fe₂O₃.CT600 as well as spent samples in the 2θ ranges (a) between 5 and 80° and (b) between 42 and 46°.

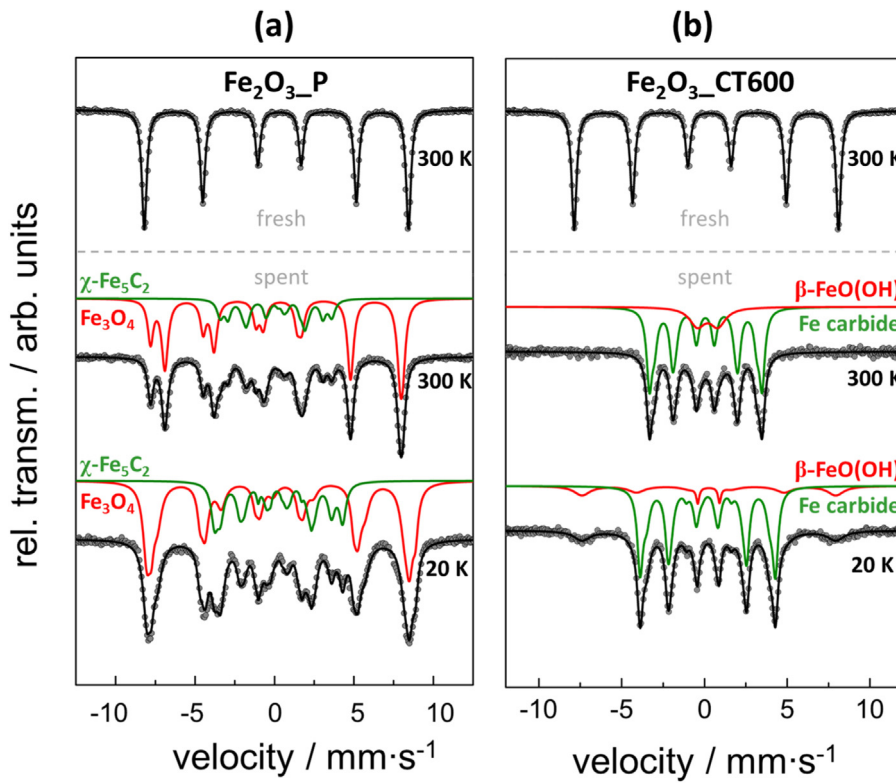


Fig. 2. Mössbauer spectra of fresh and spent (a) $\text{Fe}_2\text{O}_3\text{-P}$ and (b) $\text{Fe}_2\text{O}_3\text{-CT600}$, measured at 300 and 20 K; symbols: experimental data; lines: fit. For clarity, the sub-spectra (red: iron oxide fraction; green: iron carbide fraction) described in the text were plotted with a constant offset against the y-axis.

fresh differently prepared Fe_2O_3 catalysts strongly changed after performing $\text{CO}_2\text{-FT}$. The spent materials appear to consist of large ill-defined particles.

According to *ex situ* XRD analysis, all fresh materials are composed of the $\alpha\text{-Fe}_2\text{O}_3$ phase (Fig. S3). They, however, differ in the size of crystallites. An average crystallite size of $\text{Fe}_2\text{O}_3\text{-CT600}$ and $\text{Fe}_2\text{O}_3\text{-CT900}$ was around 75 and 100 nm respectively, while $\text{Fe}_2\text{O}_3\text{-P}$ consisted of significantly smaller crystallites of approximately 20 nm. The difference in the crystallite sizes may be responsible for the different specific surface areas of these samples (Table 1).

The effect of reaction on steady-state catalyst phase composition was also investigated by *ex situ* XRD. To this end, we characterized the catalysts used for $\text{CO}_2\text{-FT}$ at 623 K and 15 bar for 120 h on $\text{H}_2/\text{CO}_2/\text{N}_2 = 6/1/0.3$ stream (for experimental details see Section 2.3). X-ray diffractograms of these samples are illustrated in Fig. 1. No reflexes belonging to Fe_2O_3 could be detected. The main crystalline phase in all spent catalysts was found to be Fe_3O_4 with the best agreement of the pattern measured and the 2θ values of the PDF database. With a slight shift of the 2θ values, the existence of FeO(OH) is possible; both phases provide very similar XRD patterns (see Fig. S4). However, according to the below Mössbauer analysis (Fig. 2), we can conclude that Fe_3O_4 is present in $\text{Fe}_2\text{O}_3\text{-P}$ and $\text{Fe}_2\text{O}_3\text{-CT900}$, while $\text{Fe}_2\text{O}_3\text{-CT600}$ contains the $\beta\text{-FeO(OH)}$ phase. Generally, reaction-induced transformation of Fe_2O_3 is in agreement with previous studies [45,46]. Irrespective of the method of catalyst preparation, the average crystallite size of Fe_3O_4 or $\beta\text{-FeO(OH)}$ was larger than 100 nm. It is also important to highlight that Fe_5C_2 was detected in all of the spent catalysts, but with different amounts. While sample $\text{Fe}_2\text{O}_3\text{-CT600}$ contains relatively high amounts of XRD-visible iron carbide, it was just detected in traces in the other two samples (Fig. 1).

To examine the possible presence of XRD-amorphous phases in fresh and spent $\text{Fe}_2\text{O}_3\text{-P}$, $\text{Fe}_2\text{O}_3\text{-CT600}$, and $\text{Fe}_2\text{O}_3\text{-CT900}$, we

characterized these catalysts with Mössbauer spectroscopy. In agreement with XRD analysis, the only phase detected in all fresh samples was $\alpha\text{-Fe}_2\text{O}_3$, with Mössbauer parameters (see Table S1) being in good agreement with values reported in the literature [47,48]. The Mössbauer spectra of fresh $\text{Fe}_2\text{O}_3\text{-P}$ and $\text{Fe}_2\text{O}_3\text{-CT600}$ and their fits are shown in Fig. 2. The corresponding data for $\text{Fe}_2\text{O}_3\text{-CT900}$ are given in Fig. S5 and are similar to those for $\text{Fe}_2\text{O}_3\text{-P}$ in Fig. 2. In general, only marginal variations of the Mössbauer parameters were observed with respect to the different preparation methods. Therefore, the preparation method was not found to significantly affect the bulk composition of the investigated fresh catalysts.

The Mössbauer spectroscopic measurements on spent samples of $\text{Fe}_2\text{O}_3\text{-P}$ and $\text{Fe}_2\text{O}_3\text{-CT900}$ confirmed reduction of Fe_2O_3 to Fe_3O_4 under $\text{CO}_2\text{-FT}$ synthesis conditions and qualitatively corroborate the results of the XRD analysis, *i.e.* the main (crystalline) phase in these catalysts was Fe_3O_4 . The complex multiphase spectra of spent $\text{Fe}_2\text{O}_3\text{-P}$ and $\text{Fe}_2\text{O}_3\text{-CT900}$ recorded at 300 K can consistently be fitted with a model of iron in Fe_3O_4 (with two non-equivalent Fe-sites [49,50]) and iron in $\chi\text{-Fe}_5\text{C}_2$ (with three non-equivalent Fe-sites [51,52]). Furthermore, an additional component (with a volume fraction of approx. 6%), concordant with $\alpha\text{-Fe}$, has to be considered for spent $\text{Fe}_2\text{O}_3\text{-CT900}$. The application of this model resulted in a good agreement with experimental data (Figs. 2(a) and S5) and the Mössbauer parameters found are consistent with values previously reported [49–52]. This analysis allowed us to determine the ratios of Fe oxide to Fe carbide in spent $\text{Fe}_2\text{O}_3\text{-P}$ and $\text{Fe}_2\text{O}_3\text{-CT900}$ (*i.e.* the spectral area of the individual components), which were found to be 72:28 and 73:21, respectively.

The magnetically split main component of the Mössbauer spectrum of $\text{Fe}_2\text{O}_3\text{-CT600}$ measured at 300 K (Fig. 2(b)) shows neither the characteristic two component spectrum of Fe_3O_4 nor the three component spectrum of $\chi\text{-Fe}_5\text{C}_2$ (the last with a site population ratio of around 2:2:1 [51]) as found for $\text{Fe}_2\text{O}_3\text{-P}$ and

$\text{Fe}_2\text{O}_3\text{-CT900}$ (*vide supra*). Nevertheless, this spectrum was satisfactorily analyzed with two magnetically split components with Mössbauer parameters, which are consistent with iron in Fe carbide(s), however, the determined site population ratio of around 57:24 points to a mixture of different Fe carbide modifications (e.g. $\chi\text{-Fe}_5\text{C}_2$, $\epsilon'\text{-Fe}_{2.2}\text{C}$ and/or $\theta\text{-Fe}_3\text{C}$) [51–55]. Furthermore, an additional but magnetically not split component with a volume fraction of around 19% was observed (Fig. 2b) and fitted with a resolved doublet of Lorentzian lines thus suggesting the formation of (super)paramagnetic Fe oxide in spent $\text{Fe}_2\text{O}_3\text{-CT600}$. The evaluated Mössbauer parameters of this component are in agreement with values reported for iron in the β -modification of FeO(OH) [54,56,57]. This is further confirmed by a measurement performed at 20 K (Fig. 2b), revealing the development of an additional magnetic sextet with a large local magnetic hyperfine field B_{hf} of approximately 47.4 T, which is typical for iron in Fe oxide. Isomer shift, quadrupole shift and B_{hf} are furthermore consistent with $\beta\text{-FeO(OH)}$ [54,56–58].

In summary, the Mössbauer spectroscopic analysis identified Fe carbide in spent $\text{Fe}_2\text{O}_3\text{-CT600}$, $\text{Fe}_2\text{O}_3\text{-P}$ and $\text{Fe}_2\text{O}_3\text{-CT900}$. However, the catalysts strongly differ in the amount of this phase. While the $\text{Fe}_2\text{O}_3\text{-P}$ and $\text{Fe}_2\text{O}_3\text{-CT900}$ materials contain around 30 and 20% Fe carbides respectively, $\text{Fe}_2\text{O}_3\text{-CT600}$ consists of around 80% Fe carbides.

3.1.2. Catalyst reducibility

Since the reducibility of fresh iron-containing catalysts appears to be a crucial factor for their activity and selectivity in classical Fischer-Tropsch synthesis [59], we tested redox properties of our catalysts by $\text{H}_2\text{-TPR}$ measurements. The obtained $\text{H}_2\text{-TPR}$ profiles are shown in Fig. 3. They are characterized by several maxima (T_{max}) of H_2 consumption in different temperature ranges. The T_{max} values qualitatively reflect various redox processes in the course of Fe_2O_3 reduction. It is known from previous literature studies [60] that Fe_2O_3 can be reduced to metallic Fe in hydrogen via a three-step mechanism: $\text{Fe}_2\text{O}_3 \rightarrow \text{Fe}_3\text{O}_4 \rightarrow \text{FeO} \rightarrow \text{Fe}^0$. This order follows rising reduction temperature. The $\text{H}_2\text{-TPR}$ profiles in Fig. 3 are characterized by three T_{max} indicating that the above reduction sequence is also valid for reduction of our samples. They, however, differ in the temperature of the first reduction step. The $\text{H}_2\text{-TPR}$ profile of $\text{Fe}_2\text{O}_3\text{-CT600}$ is characterized by the lowest T_{max} value of 655 K. The corresponding value for $\text{Fe}_2\text{O}_3\text{-P}$ was 673 K. Since these both fresh materials were calcined at the same temperature of 873 K, we can conclude that the cellulose-templated method yielded Fe_2O_3 with easier reducibility. In addition, calcination temperature in this method is an important factor affecting Fe_2O_3 reducibility as concluded from the significantly higher T_{max} value of 740 K for the first reduction step in $\text{Fe}_2\text{O}_3\text{-CT900}$. This result is in agreement with previous studies of redox properties of Ce-Fe mixed oxides [61].

In summary, the results of material characterization revealed that phase transformation of initial Fe_2O_3 after CO_2 hydrogenation tests and redox properties of fresh Fe_2O_3 are strongly affected by catalyst preparation method. To evaluate the impact onto catalytic properties, we tested differently synthesized Fe_2O_3 catalysts for their activity and selectivity in $\text{CO}_2\text{-FT}$. The results are presented and discussed in the next section.

3.2. Catalytic performance and comparison with the state of the art

To ensure a conclusive benchmarking of our samples with respect to the state of the art Fe-based catalysts previously used for $\text{CO}_2\text{-FT}$, their performance should be compared under the same reaction conditions. After analyzing available data about $\text{CO}_2\text{-FT}$ [27,28,30,33,35,36], the following reaction conditions appear to be

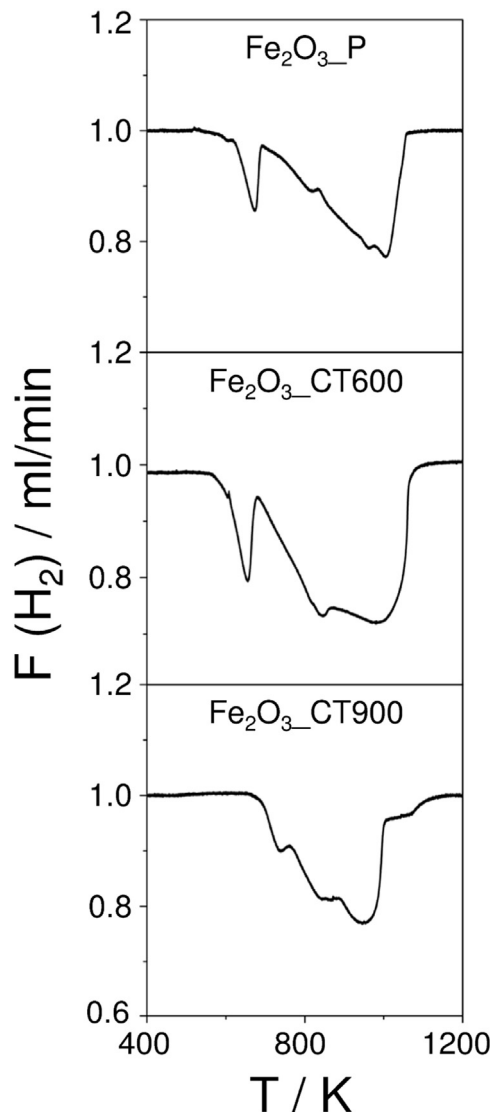


Fig. 3. $\text{H}_2\text{-TPR}$ profiles of fresh iron oxides.

the most frequently used in literature: reaction temperature of 573 K, total pressure of 10 bar and H_2/CO_2 ratio of 3. Therefore, these reaction parameters were also selected for a first series of catalytic tests in this study. GHSV was varied to achieve a steady-state CO_2 conversion between 20 and 25%. It is also worth mentioning that the data we report were obtained after catalyst activation phase, which is typical for materials used for $\text{CO}_2\text{-FT}$ synthesis. The detected carbon-containing gas-phase reaction products in this test were CO , CH_4 (non-desired product) and desired C_{2+} hydrocarbons with a chain length up to C_{18} . From the results shown in Table 2, one can see that the method of Fe_2O_3 preparation has a decisive effect on the selectivity to the desired products. The highest C_{2+} selectivity of 65% was obtained over $\text{Fe}_2\text{O}_3\text{-CT600}$ at a CO_2 conversion of about 23%, while the $\text{Fe}_2\text{O}_3\text{-CT900}$ catalysts showed only 35% C_{2+} selectivity at a similar degree of CO_2 conversion. The corresponding values for methane selectivity were around 14 and 36%. The $\text{Fe}_2\text{O}_3\text{-P}$ catalyst was less selective in terms of C_{2+} hydrocarbons than $\text{Fe}_2\text{O}_3\text{-CT600}$ but performed superior to $\text{Fe}_2\text{O}_3\text{-CT900}$.

As seen in Table 2 our best performing $\text{Fe}_2\text{O}_3\text{-CT600}$ catalyst showed comparable or even superior performance to the state of the art materials. Importantly, the latter materials were doped with different promoters to achieve high C_{2+} selectivity, while our catalyst was not promoted. Thus, $\text{CO}_2\text{-FT}$ synthesis performance of

Table 2

Conversion (X) of CO₂, olefin to paraffin ratio (O/P) among C₂–C₄ hydrocarbons, and selectivity (S) to C₂₊ hydrocarbons obtained over present and various state of the art Fe-based catalysts at 10 bar and 573 K using a feed with the ratio of H₂/CO of 3.

Catalyst	X(CO ₂)/%	S(C ₂₊)/%	S(CH ₄)/%	F/m _{cat} /mL/(g·h)	O/P	Refs.
Fe ₂ O ₃ -P	18	47	37	1140	0.1	present
Fe ₂ O ₃ -CT600	23	65	14	1140	1.4	present
Fe ₂ O ₃ -CT900	21	35	36	1140	0.2	present
Fe/NaY	21	59	10	1900	1.5	[33]
Fe-K/Al ₂ O ₃	31	69	8	1800	6.1	[36]
Fe-Cu-K-Al	41	80	14	1800	3.8	[28]
Fe-K/Al ₂ O ₃	35	67	12	2000	1.1	[35]
FeCeO _x	25	40	38	15500	—	[27]
Fe-La-Cu-K/Al ₂ O ₃	32	65	20	1320	0.2	[30]
Fe-Ru-Mn-K/Al ₂ O ₃	30	64	19	1320	1.6	[30]
Fe-Mn-Cu-Zn-K/TiO ₂	23	50	9	1320	1.0	[30]
Fe-Mg-Cu-K/Al ₂ O ₃	29	62	22	1320	0.5	[30]
Fe-Zr-Mn-Cu-K/TiO ₂	26	49	8	1320	3.2	[30]
Fe-Zr-Cu-K/TiO ₂	25	48	6	1320	4.0	[30]

bare Fe₂O₃, which is typically considered to be unselective in the target reaction, can be significantly improved when using a proper method for its preparation.

To further elucidate the potential of Fe₂O₃-CT600 for CO₂-FT synthesis, we performed an additional test at 15 bar over 280 h on stream under different reaction conditions. Reaction temperature was varied between 573 and 673 K, while the ratio of H₂/CO₂ was 3 or 6. The test was started at 673 K using a feed with the H₂/CO₂ ratio of 6. After reaching a steady-state operation, reaction conditions were changed until a new steady-state performance was achieved.

Fig. 4 shows CO₂ conversion over Fe₂O₃-CT600 as well as selectivity to CH₄, C₂₊, and CO as a function of time on stream under different reaction conditions. We shall start with the discussion of catalyst on-stream stability. The conversion was stable over 30–50 h on stream under a certain reaction condition (see Fig. 4). The data points obtained within the first and last 50 h on stream (under the same reaction condition) also indicate that the catalyst did practically not lose its activity over the whole time scale of the test of 280 h. However, some changes in product selectivity were observed. The initial (within the first 50 h) selectivity to CH₄ was around 21 and 12% using feeds with the ratio of H₂/CO of 6 and 3, respectively. The corresponding values at the end of the test (after 280 h) were 30 and 18%. The selectivity to C₂₊-hydrocarbons was decreased by the same extent, while CO selectivity remained constant.

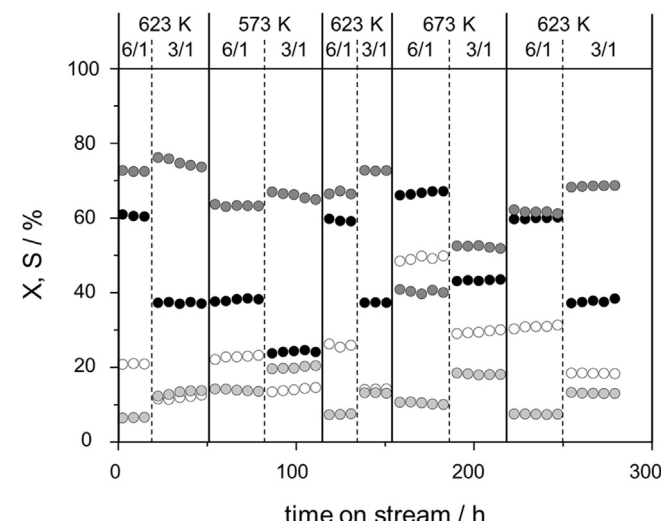


Fig. 4. Conversion (X) of CO₂ (●) and selectivity (S) to C₂₊ hydrocarbons (●), CO (○) and CH₄ (○) over Fe₂O₃-CT600 at different temperatures and H₂/CO₂ ratio (6/1 or 3/1) in feed; P = 15 bar, τ = 1.0 g min/l.

In the following, we discuss the effects of temperature and H₂/CO₂ ratio on catalytic performance. As expected, CO₂ conversion increased with rising temperature and H₂/CO₂ ratio. It is important to mention that CH₄ selectivity did not practically change with an increase in temperature from 573 to 623 K despite the conversion increased from 23 to 40% and from 40 to 60% for feeds with the ratio of H₂/CO of 3 and 6, respectively. The corresponding changes in the selectivity to C₂₊-hydrocarbons were from 65 to 70% and from 62 to 66%, while CO selectivity decreased (from 20 to 12% for H₂/CO = 3 feed; 13 to 8% for H₂/CO = 6 feed) at higher reaction temperatures. This indicates that FT activity of Fe₂O₃-CT600 to form C₂₊ is increased at 623 K. For both feeds, the selectivity to CH₄ increased with a further increase in temperature to 673 K, while the desired selectivity decreased accordingly.

Under the above consideration, the best catalytic results regarding high CO₂ conversion and low CH₄ selectivity were obtained at 623 K. The highest overall yield of C₂₊ hydrocarbons was around 40% with a reactant feed of H₂/CO₂ = 6; the corresponding selectivity was 66% at 60% CO₂ conversion. A change of the reactant feed to H₂/CO₂ = 3 resulted in a lower yield of 27% with the selectivity to C₂₊-hydrocarbons of 73%. On the other hand, the selectivity to methane also strongly decreased from around 20 to 12% with declining H₂/CO₂ ratio from 6 to 3. CO selectivity was found to be significantly higher at feed 3, due to the lower hydrogen partial pressure in this feed.

For further evaluating the effect of feed composition on catalytic performance we calculated chain-growth probability α and olefin fraction at 623 K. It was found, that the chain growth probability increased from 52% to 70% with a decrease in the H₂/CO₂ ratio from 6 to 3 due to lower hydrogen partial pressure. The hydrogenation of olefins to the corresponding alkanes is also suppressed at lower hydrogen partial pressure. As a consequence, the olefin to paraffin ratio among C₂–C₄ hydrocarbons increased from 1.2 to 2.7 when replacing the H₂/CO₂ = 6 feed by the H₂/CO₂ = 3 feed. In comparison with these beneficial effects of a lowered H₂/CO₂ ratio, CO₂ conversion unfortunately dropped from 59 to 37%. As a consequence, an overall yield of C₂–C₄ olefins decreased from 12 to 9%.

3.3. Effect of catalyst preparation method on pathways of product formation in CO₂-FT

For understanding fundamental origins of the effect of preparation method of Fe₂O₃ on catalytic performance in CO₂-FT synthesis, deeper insights into individual reaction steps and their kinetics are needed. Therefore, we performed catalytic tests at different GHSV to achieve different degrees of CO₂ conversion; the lower the GHSV, the higher the conversion is. The idea was to investigate how the selectivity to CO, CH₄ and C₂₊ hydrocarbons is influenced by the

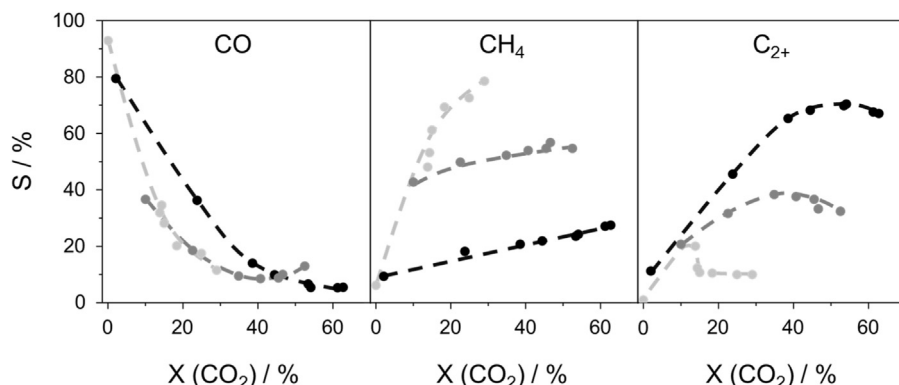


Fig. 5. Selectivity (S) to CO, CH₄, and C₂₊ hydrocarbons versus conversion (X) of CO₂ over Fe₂O₃.P (●), Fe₂O₃.CT600 (●) and Fe₂O₃.CT900 (●). Reaction conditions: 623 K, 15 bar, H₂/CO₂/N₂ = 6/1/0.3.

conversion. The obtained selectivity-conversion relationships are shown in Fig. 5. It should be particularly stressed that the experimental data in this figure were obtained after a pseudo steady-state operation was achieved.

For all catalysts, non-zero CO selectivity will be achieved at a zero conversion of CO₂. Therefore, it can be assumed that CO is directly formed from CO₂ through the RWGS reaction as had been documented in previous studies of CO₂-FT over different Fe-based catalysts [62,63]. For all catalysts, the selectivity to CO decreases with rising CO₂ conversion, while the selectivity to CH₄ and C₂₊-hydrocarbons increases. Such dependence suggests that the latter products are formed from CO through classical CO-FT synthesis reaction pathways. C₂₊ hydrocarbons can also be converted into CH₄ through their hydrogenolysis. This reaction gained importance with rising CO₂ conversion (see maxima in the C₂₊ selectivity profiles in Fig. 5). The following order of hydrogenolysis activity was found: Fe₂O₃.P > Fe₂O₃.CT900 > Fe₂O₃.CT600. The method of Fe₂O₃ preparation also affected another pathway of CH₄ formation as discussed below.

The RWGS reaction is not the only direct pathway of CO₂ conversion because the primary (at zero degree of CO₂ conversion) selectivity to CO is not 100% over all catalysts. It is clearly seen in Fig. 5 that non-zero methane selectivity is predicted at zero CO₂ conversion. This means that CO₂ should be directly (without intermediate formation of CO) hydrogenated to CH₄. Fe₂O₃.CT900 was concluded to show the highest activity to promote this reaction because CH₄ selectivity of around 40% is expected at zero CO₂ conversion (Fig. 5). For all catalysts, this undesired hydrocarbon was also formed through hydrogenation of CO. This conclusion was made on the basis of the fact that CH₄ selectivity increased with CO₂ conversion, while CO selectivity decreased (Fig. 5). Importantly, the catalysts strongly differ in their activity for this non-desired reaction pathway as evident from different slopes of the CH₄ selectivity profile. The Fe₂O₃.P catalysts showed the highest activity, while both cellulose-templated catalysts were significantly less active and performed similar to each other.

Under consideration of the above discussion of the selectivity-conversion relationships in Fig. 5, we suggest the following overall scheme of product formation in the course of CO₂-FT synthesis (Fig. 6). CO and CH₄ are the only primary products, while C₂₊ hydrocarbons are exclusively formed through CO hydrogenation. These hydrocarbons can also be converted to CH₄ at low GHSV. The latter alkane is additionally formed from CO even at high GHSV. The determined scheme is in accordance with other previous studies [21,64], where similar reaction steps were observed in CO₂ hydrogenation over Fe-based catalysts. All these reaction pathways appear to be affected by the method of Fe₂O₃ preparation. Connecting the catalyst characterization data (Section 3.1) to the presented catalytic

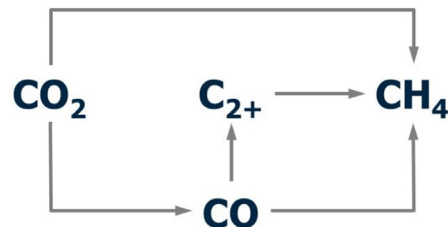


Fig. 6. Pathways of CO₂ conversion into detected reaction products.

results, it can be concluded that the most catalytically relevant property influenced by the preparation method is reducibility of the resulting materials. This property plays an important role in in-situ transformation of Fe₂O₃ to iron carbides. Owing to an improved reducibility of the Fe₂O₃.CT600, significant amounts of Fe carbide (Table 1) were formed under reaction conditions. Iron carbides are known to be an active phase in CO-based Fischer-Tropsch synthesis and to be responsible for chain growth. In agreement, iron carbide containing catalysts showed the highest selectivity to C₂₊ hydrocarbons and the lowest activity for CO/CO₂ hydrogenation to CH₄.

In summary, the present study revealed that non-desired CH₄ formation could be significantly suppressed even at high degrees of CO₂ conversion without using any promoters for Fe₂O₃. Under this consideration, it is expected that catalytic performance can be further improved by more detailed knowledge about the effects of the presented synthesis method. To this end, deep understanding of factors governing the kinetics of activation of CO₂, CO and H₂ is still required.

4. Conclusions

Bare Fe₂O₃ derived from Fe(NO₃)₃ through a cellulose-templated (CT) synthesis method produced higher alkanes and olefins from CO₂ with a selectivity higher or close to that of the state of the art Fe-based materials, which must, however, be promoted with e.g. K, Cu, Mn or Ru to perform selectively. The unique role of the CT-synthesized catalyst precursor is its easier reduction and in-situ conversion to iron carbide, the active phase for FT synthesis.

An overall scheme of CO₂ hydrogenation did not depend on steady-state catalyst phase composition with the latter, however, influencing the kinetics of selective and non-selective reaction pathways. Both direct CO₂ methanation and conversion of CO and desired hydrocarbons into CH₄ were concluded to be strongly suppressed over the CT-derived sample. The obtained results provide new insights required for the design of CO₂-hydrogenation cat-

alysts and open possibilities for tuning their selectivity in terms of suppressing undesired CH₄ formation in favor of short-chain olefins.

Acknowledgement

The authors would like to thank Prof. Dr. F.J. Litterst (Institut für Physik der Kondensierten Materie) at the TU Braunschweig for providing access to the (continuous flow cryostat) ⁵⁷Fe-Mössbauer spectrometer.

Appendix A. Supplementary data

Supplementary data associated with this article can be found, in the online version, at <http://dx.doi.org/10.1016/j.apcatb.2016.11.017>.

References

- [1] M.K. Van Aalst, Disasters 30 (2006) 5–18.
- [2] J.T. Kiehl, K.E. Trenberth, Bull. Am. Meteorol. Soc. 78 (1997) 197–208.
- [3] Y. Li, B. Zou, C.W. Hu, M.H. Cao, Carbon 99 (2016) 79–89.
- [4] J. Kemper, Int. J. Greenhouse Gas Control 40 (2015) 401–430.
- [5] D.Y.C. Leung, G. Caramanna, M.M. Maroto-Valer, Renew. Sust. Energ. Rev. 39 (2014) 426–443.
- [6] E.V. Kondratenko, G. Mul, J. Baltrusaitis, G.O. Larrazabal, J. Perez-Ramirez, Energy Environ. Sci. 6 (2013) 3112–3135.
- [7] B. Hu, C. Guild, S.L. Suib, J. CO₂ Util. 1 (2013) 18–27.
- [8] A.T. Najafabadi, Int. J. Energy Res. 37 (2013) 485–499.
- [9] J.M. Zhang, J. Sun, X.C. Zhang, Y.S. Zhao, S.J. Zhang, Greenhouse Gases: Sci. Technol. 1 (2011) 142–159.
- [10] I. Ganesh, Renew. Sust. Energ. Rev. 59 (2016) 1269–1297.
- [11] A.C. Kathalikkattil, R. Babu, J. Tharun, R. Roshan, D.-W. Park, Catal. Surv. Asia 19 (2015) 223–235.
- [12] Y. Demirel, M. Matzen, C. Winters, X. Gao, Int. J. Energ. Res. 39 (2015) 1011–1047.
- [13] M. Marszewski, S.W. Cao, J.G. Yu, M. Jaroniec, Mater. Horiz. 2 (2015) 261–278.
- [14] A.H. Liu, B. Yu, L.N. He, Greenhouse Gases: Sci. Technol. 5 (2015) 17–33.
- [15] V.N. Nguyen, L. Blum, Chem. Ing. Tech. 87 (2015) 354–375.
- [16] S. Roensch, J. Schneider, S. Matthischke, M. Schlueter, M. Goetz, J. Lefebvre, P. Prabhakaran, S. Bajohr, Fuel 166 (2016) 276–296.
- [17] J. Gao, Q. Liu, F. Gu, B. Liu, Z. Zhong, F. Su, RSC Adv. 5 (2015) 22759–22776.
- [18] M.D. Porosoff, B.H. Yan, J.G.G. Chen, Energy Environ. Sci. 9 (2016) 62–73.
- [19] S.S. Geng, F. Jiang, Y.B. Xu, X.H. Liu, ChemCatChem 8 (2016) 1303–1307.
- [20] N. Fischer, R. Henkel, B. Hettel, M. Iglesias, G. Schaub, M. Claeys, Catal. Lett. 146 (2016) 509–517.
- [21] T. Riedel, G. Schaub, K.-W. Jun, K.-W. Lee, Ind. Eng. Chem. Res. 40 (2001) 1355–1363.
- [22] S.R. Yan, K.W. Jun, J.S. Hong, M.J. Choi, K.W. Lee, Appl. Catal. A 194 (2000) 63–70.
- [23] R.W. Dorner, D.R. Hardy, F.W. Williams, H.D. Willauer, Catal. Commun. 15 (2011) 88–92.
- [24] D. Mattia, M.D. Jones, J.P. O'Byrne, O.G. Griffiths, R.E. Owen, E. Sackville, M. McManus, P. Plucinski, ChemSusChem 8 (2015) 4064–4072.
- [25] T. Suzuki, K. Saeki, Y. Mayama, T. Hirai, S. Hayashi, React. Kinet. Catal. Lett. 44 (1991) 489–497.
- [26] M. Fujiwara, R. Kieffer, H. Ando, Q. Xu, Y. Souma, Appl. Catal. A 154 (1997) 87–101.
- [27] F.J. Perez-Alonso, M. Ojeda, T. Herranz, S. Rojas, J.M. Gonzalez-Carballo, P. Terreros, J.L.G. Fierro, Catal. Commun. 9 (2008) 1945–1948.
- [28] J.-S. Hong, J.S. Hwang, K.-W. Jun, J.C. Sur, K.-W. Lee, Appl. Catal. A 218 (2001) 53–59.
- [29] J.L. Zhang, S.P. Lu, X.J. Su, S.B. Fan, Q.X. Ma, T.S. Zhao, J. CO₂ Util. 12 (2015) 95–100.
- [30] U. Rodemerck, M. Holeňa, E. Wagner, Q. Smejkal, A. Barkschat, M. Baerns, ChemCatChem 5 (2013) 1948–1955.
- [31] S.-S. Nam, G. Kishan, M.-J. Choi, K.-W. Lee, Greenhouse Gas Control Technologies 4, Elsevier Science Ltd, Oxford, 1999, pp. 415–420.
- [32] R.W. Dorner, D.R. Hardy, F.W. Williams, H.D. Willauer, Appl. Catal. A 373 (2010) 112–121.
- [33] S.-S. Nam, H. Kim, G. Kishan, M.-J. Choi, K.-W. Lee, Appl. Catal. A 179 (1999) 155–163.
- [34] M. Fujiwara, R. Kieffer, H. Ando, Y. Souma, Appl. Catal. A 121 (1995) 113–124.
- [35] S.C. Lee, J.H. Jang, B.Y. Lee, M.C. Kang, M. Kang, S.J. Choung, Appl. Catal. A 253 (2003) 293–304.
- [36] J.S. Hwang, K.W. Jun, K.W. Lee, Appl. Catal. A 208 (2001) 217–222.
- [37] R.E. Owen, J.P. O'Byrne, D. Mattia, P. Plucinski, S.I. Pascu, M.D. Jones, ChemPlusChem 78 (2013) 1536–1544.
- [38] D.-B. Cao, Y.-W. Li, J. Wang, H. Jiao, J. Mol. Catal. A 346 (2011) 55–69.
- [39] E. de Smit, F. Cinquini, A.M. Beale, O.V. Safonova, W. van Beek, P. Sautet, B.M. Weckhuysen, J. Am. Chem. Soc. 132 (2010) 14928–14941.
- [40] E. de Smit, B.M. Weckhuysen, Chem. Soc. Rev. 37 (2008) 2758–2781.
- [41] C. Berger-Karin, E.V. Kondratenko, Stud. Surf. Sci. Catal. 175 (2010) 635–638.
- [42] C. Berger-Karin, S. Wohlrab, U. Rodemerck, E.V. Kondratenko, Catal. Commun. 18 (2012) 121–125.
- [43] A.N. Shigapov, G.W. Graham, R.W. McCabe, H.K. Plummer, Appl. Catal. A 210 (2001) 287–300.
- [44] V. Gölden, S. Sokolov, V.A. Kondratenko, E.V. Kondratenko, Appl. Catal. B 101 (2010) 130–136.
- [45] S.Z. Li, G.D. Meitzner, E. Iglesia, J. Phys. Chem. B 105 (2001) 5743–5750.
- [46] D.L. Fu, W.W. Dai, X.C. Xu, W. Mao, J.J. Su, Z.P. Zhang, B.F. Shi, J. Smith, P. Li, J. Xu, Y.F. Han, ChemCatChem 7 (2015) 752–756.
- [47] O.C. Kistner, A.W. Sunyar, Phys. Rev. Lett. 4 (1960) 412–415.
- [48] F. van der Woude, Phys. Status Solidi B 17 (1966) 417–432.
- [49] R. Bauminger, S.G. Cohen, A. Marinov, S. Ofer, E. Segal, Phys. Rev. 122 (1961) 1447–1450.
- [50] S.K. Banerjee, W. O'Reilly, C.E. Johnson, J. Appl. Phys. 38 (1967) 1289–1290.
- [51] G. Le Caer, J.M. Dubois, J.P. Senateur, J. Solid State Chem. 19 (1976) 19–28.
- [52] X.-W. Liu, S. Zhao, Y. Meng, Q. Peng, A.K. Dearden, C.-F. Huo, Y. Yang, Y.-W. Li, X.-D. Wen, Sci. Rep. 6 (2016) 26184.
- [53] J.A. Amelse, J.B. Butt, L.H. Schwartz, J. Phys. Chem. 82 (1978) 558–563.
- [54] J.A. Amelse, G. Grynkewich, J.B. Butt, L.H. Schwartz, J. Phys. Chem. 85 (1981) 2484–2488.
- [55] B. David, O. Schneeweiss, M. Mashlan, E. Šantavá, I. Morjan, J. Magn. Magn. Mater. 316 (2007) 422–425.
- [56] M.J. Rossiter, A.E.M. Hodgson, J. Inorg. Nucl. Chem. 27 (1965) 63–71.
- [57] I. Dézsi, L. Keszthelyi, D. Kuligawczuk, B. McInár, N.A. Eissa, Phys. Status Solidi B 22 (1967) 617–629.
- [58] T. Takada, M. Kiyama, Y. Bando, T. Nakamura, M. Shiga, T. Shinjo, N. Yamamoto, Y. Endoh, H. Takaki, J. Phys. Soc. Jpn. 19 (1964) (1744–1744).
- [59] S.-H. Kang, J.W. Bae, P.S. Sai Prasad, S.-J. Park, K.-J. Woo, K.-W. Jun, Catal. Lett. 130 (2009) 630–636.
- [60] W.K. Jozwiak, E. Kaczmarek, T.P. Maniecki, W. Ignaczak, W. Maniukiewicz, Appl. Catal. A 326 (2007) 17–27.
- [61] K. Li, H. Wang, Y. Wei, D. Yan, Int. J. Hydrogen Energy 36 (2011) 3471–3482.
- [62] D.H. Kim, S.W. Han, H.S. Yoon, Y.D. Kim, J. Ind. Eng. Chem. 23 (2015) 67–71.
- [63] A.G. Kharaji, A. Sharifi, M.A. Takassi, Chinese J. Chem. Eng. 21 (2013) 1007–1014.
- [64] R. Satthawong, N. Koizumi, C. Song, P. Prasassarakich, Catal. Today 251 (2015) 34–40.